### Template for Submission of Manuscripts to American Chemical Society Journals Word 2010, Page Wide Abstract Version



# Using Iodine as a dopant for metal-radical materials to investigate possible charge-transfer salts.

JENNIFER GARNER CHEM\*4910 CHEMISTRY RESEARCH PROJECT

SUPERVISOR: PROFESSOR KATHRYN PREUSS

**FALL 2016** 

## Using Iodine as a dopant for metal-radical materials to investigate possible charge-transfer salts.

Jennifer Garner\*

Department of Chemistry, University of Guelph, 50 Stone Road East, Guelph, Ontario, NiG 2W1, Canada KEYWORDS: molecule-based magnet, charge-transfer salt, Peierls distortion, metal-radical approach, organic radical, pancake bonding, dimerization, differential scanning calorimetry, powder x-ray diffraction.

**ABSTRACT:** This paper is the second installment of the project, and it discusses the combination of charge transfer with molecule-based magnet materials. An introduction to molecule-based materials, magnetism, and conductivity is given, followed by an explanation of charge transfer salts (as being the inspiration for the project). An example synthesis for a DTDA radical as conducted by the student is shown, along with possible mechanistic steps. The choice of metals for the intended complexes for iodine-doping is explained. P-doping is a proposed manner of incurring conductance in metal-radical complexes. It has the potential to prevent the dimerization that can occur through pancake bonding. Grinding iodine with the Ni-pyDTDA metal-radical complex and heating through DSC seems to produce a new compound, which suggests that this is a good screening method for p-doping of metal-radical materials. PXRD is also shown to help characterize starting materials.

Molecule design is of interest to chemists who would like to apply certain functionalities to their compounds. The chemist's "synthetic toolkit" can be used to find chemical pathways for a molecule of interest, and to provide the functional groups and geometries to enable such characteristics as conductivity, magnetism, volatility, solubility, luminescence, etc. Compared to bulk materials, it is easy to determine the purity and exact structure of moleculebased materials using the many known spectrographic and analytical techniques. In this paper, the possibility of generating materials with both conductive and magnetic properties will be explored. Given a magnetic and conductive molecule, how does the bulk phase behave, and how can the possible magnetic and conductive interactions be used to explain key concepts about the nature of chemical bonding, electricity, and magnetism?

The term "metal-radical approach" was first used by Caneschi, Getteschi, Sessoli, and Rey in 1989. It describes the use of a paramagnetic ligand to facilitate magnetic coupling between two paramagnetic metal centres. The metal-radical approach can generate molecular magnetic materials that possess spontaneous magnetization below a critical temperature.

Without the metal-radical approach, use of a diamagnetic ligand between metal centres makes it more difficult to achieve a non-zero magnetic moment as this requires breaking symmetry. Usually, the spins of identical metals will oppose one another, resulting in a magnetic moment of zero (Figure 1) and repulsion in the presence of a magnetic field. Breaking symmetry is a topic of interest to organic and biological chemists, especially with regards to

chiral structures.<sup>2,3</sup> Also, breaking symmetry – for example removing an inversion centre – is explored by materials scientists who want to use polarization for capacitors and actuators, and for the magnetically ordered states (antiferroand ferromagnetism) that could have applications in data storage.<sup>5</sup> Breaking symmetry can be accomplished by using two different metal centres, or metal centres with distinct oxidation states. Another way to break symmetry is by using an asymmetric ligand that exhibits unique interaction/orbital overlap with each metal; however, it is synthetically more challenging to design and construct asymmetric ligands compared to symmetric ligands.<sup>6</sup>

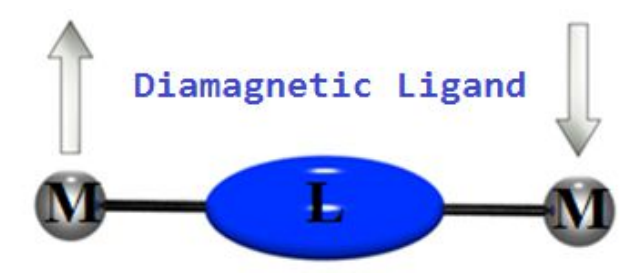


Figure 1. The use of a diamagnetic ligand between two identical metal centres will most likely result in opposing spins for the metals and thus a magnetic moment of zero.

The metal-radical approach allows for two possibilities (Figure 2); the spin states of the metals and the ligand align for ferromagnetic coupling (non-zero spin ground state, S=1), or the spin state of the metals is opposite to that of the spin state for the ligand for anti-ferromagnetic coupling (zero spin ground state, S=0). The type of coupling is

thus determined by the spin ground state of the metal relative to the ligand and the symmetry of the overlapping orbitals.

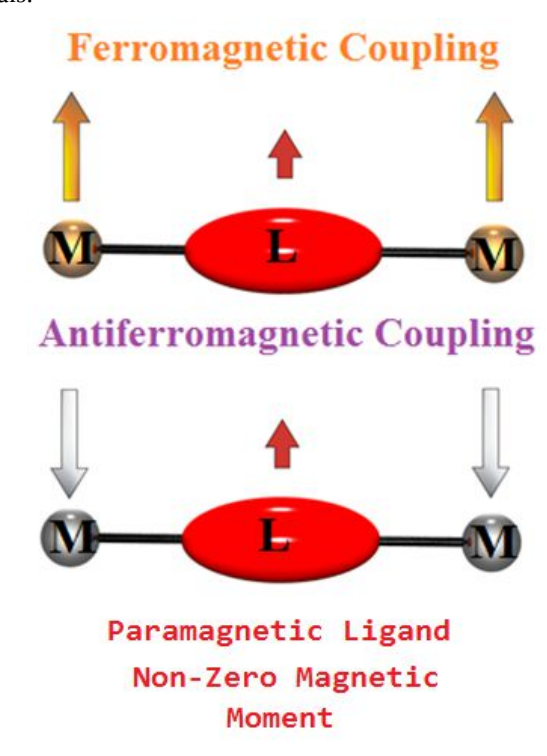


Figure 2. Use of a paramagnetic ligand can facilitate magnetic coupling between two paramagnetic metal centres such that there is a non-zero magnetic moment. The two types of coupling are –*Top*- ferromagnetic (ground spin state is non-zero), and –*Bottom*- antiferromagnetic (ground spin state is zero).

The chosen paramagnetic ligands for this work are thiazyl radicals, which contain -[S•=N]-.7.8 Another group of paramagnetic species is based on the nitroxyl radical =[N-O•], but nitroxyl radicals do not coordinate well to metal centres compared to thiazyl radicals.<sup>9,10</sup> Instead, nitroxyl radicals are used mainly for oxidation studies, spin-labelling, catalysis, and electrochemistry.11,12 Examples of nitroxyl radicals are in Figure 3. Comparing the physical properties of NO versus SN, which are isoelectronic analogues of one another, NO is a colourless gas and SN cannot be isolated in the gas phase except at low temperatures.<sup>7,8</sup> With regards to reactivity, SN can form polymers and heterocycles of various sizes, but NO does not catenate easily.<sup>7,8</sup> Poly(sulphur nitride) exhibits metallic and superconducting properties, and so thiazyl radicals are likely a good starting material for imparting molecules with magnetism and conductivity.

Thiazyl radicals are not air- or moisture-stable; however, they are stable in the solid state and in dry organic solvents. Stable here means that the radicals can be stored in an inert atmosphere without decomposing or undergoing some form of self-reaction.<sup>7</sup> To work with these compounds, knowledge of Schlenk line and glovebox techniques, as well as air-sensitive sample preparation techniques, are

needed. Some examples of thiazyl radicals are in Figure 4. The main thiazyl radicals of interest for this research are based on the 1,2,3,5-dithiadiazolyl moiety, which will henceforth be shortened to DTDA.

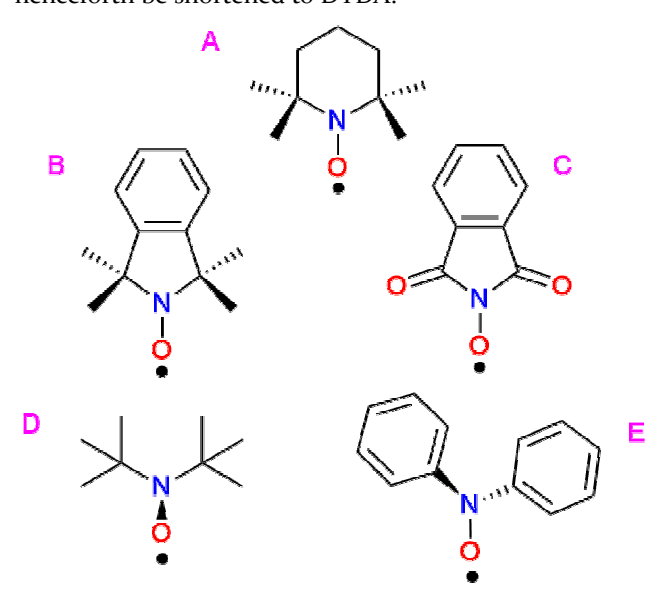


Figure 3. Some examples of organic nitroxyl radicals.<sup>12</sup> (A) 2,2,6,6-tetramethylpiperidinyloxyl or TEMPO, (B) TEMINO, (C) diacylnitroxyl or phthalimide-N-oxyl (PINO) radical, (D) di-*tert*-butylnitroxyl, and (E) N,N-diphenylnitroxyl.

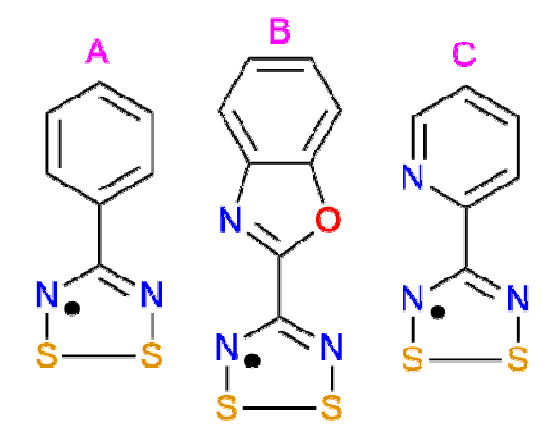


Figure 4. Examples of thiazyl radicals as pertaining to this work. Note the common DTDA heterocycle present in each. (A) 4-phenyl DTDA or phDTDA, (B) 4-(benzoxazol-2'-yl) DTDA or boaDTDA, and (C) 4-(z'-pyridyl) DTDA or pyDTDA.

Synthesis of DTDA radicals can be achieved using a nitrile R group precursor (Scheme 1). For example, to make 4-(2'-pyridyl) DTDA or pyDTDA, the starting material is 2-Pyridinecarbonitrile. Last semester, the student completed the synthesis of the benzoxazole DTDA or boaDTDA. This semester, the student synthesized pyDTDA using the known procedure<sup>18</sup>, as it was necessary to use for measurements of radical starting materials.

Scheme 1. Synthesis of the DTDA heterocycle starting from the nitrile precursor. Examples of R can be pyridyl, phenyl, and benzoxazole. Me = CH<sub>3</sub>.

$$R = N = \frac{1. \text{LiN(SiMe}_3)_2 \cdot \text{Et}_2\text{O, Toluene}}{2. \text{SiMe}_3\text{Cl, } \Delta, \text{Toluene}} R = \frac{N(\text{SiMe}_3)}{N(\text{SiMe}_3)_2} \times S_2\text{Cl}_2 \times S_2\text{Cl}_2$$

$$R = \frac{N-S}{N-S} = \frac{1/2 \text{SbPh}_3}{A \text{cetonitrile}} R = \frac{N-S}{N-S} \times \frac{N-S}{N-S}$$

The radical synthesis was performed under inert argon atmosphere using a Schlenk line. All solvents used in the radical synthesis were from the solvent purification system (SPS) in the Preuss lab, which ensured that the solvents were dry. 2-pyridinecarbonitrile (2.7836g, 26.73mmol) and lithium bis(trimethylsilyl)amide ethoxyethane  $(LiN(Si(CH_3)_3)_2 \cdot Et_2O, 6.2980g, 26.08mmol)$  were mixed for 3 hours in toluene to give a clear, yellow solution. Trimethylsilyl chloride (Si(CH<sub>3</sub>)<sub>3</sub>Cl, 3.3mL, 25.83mmol) was added to the solution, which subsequently turned opaque yellow. This solution was gently heated overnight, filtered to remove LiCl, and then the solvent was evaporated to afford a yellow/green-brown oil. The crude amidine was distilled (5.4570g, 16.16mmol, 62.59% yield) and then reacted with excess sulphur monochloride (S<sub>2</sub>Cl<sub>2</sub>, 5.2mL, 65mmol) in acetonitrile to produce the chloride salt (crude yield >100%, 3.7580g, 17.26mmol). Lastly, the crude chloride salt (3.7430g, 17.19mmol) was reacted with a half-equivalent of triphenyl antimony (SbPh3, 3.0549g, 8.652mmol) in acetonitrile for a dark black solution. This solution was filtered to obtain the radical, which was sublimed at 80°C to give dark green crystals (sublimed yield 10.92%, 0.3420g, 1.877mmol). A proposed mechanism for this synthesis is shown Figures 5-7.

The synthesis of the chloride salt (Figure 6) requires an excess of sulphur monochloride and, for reasons yet to be discovered, does not proceed in a stoichiometric fashion. The crystal structure for this chloride salt is interesting in that the chloride exhibits both covalent and ionic bonding characteristics. The covalent bonding nature may explain why the chloride salt is partially soluble in organic, nonpolar solvents. As shown in Figure 7, the reduction of the chloride salt uses a half-equivalent of SbPh<sub>3</sub>, because SbPh<sub>3</sub> is a two-electron oxidizing agent and has stable oxidation states of III and V.

4-(2'-pyridyl)-N,N,N'-tris(trimethylsilyl)amidine

Figure 5. Starting from the nitrile, shows the proposed mechanism for the synthesis of the pyridyl amidine.

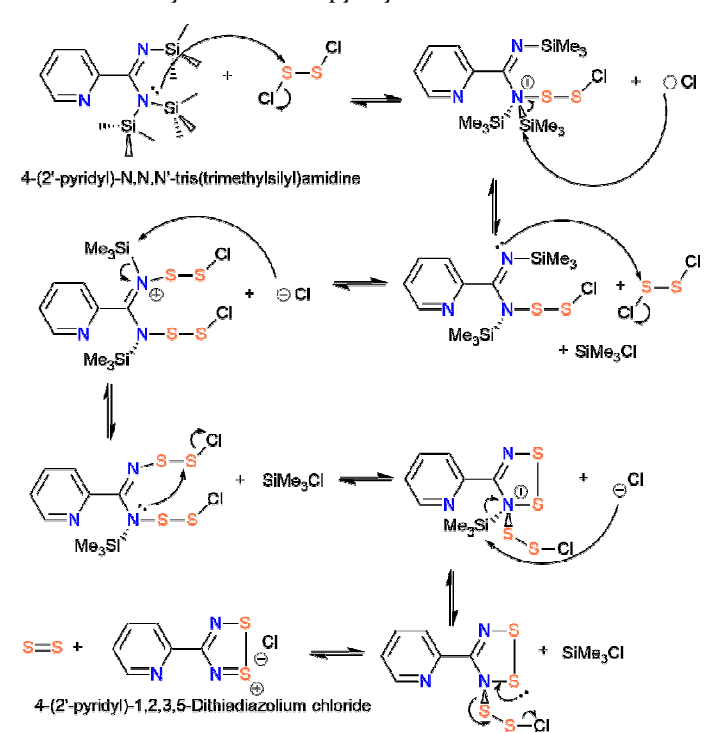


Figure 6. Starting from the pyridyl amidine, shows the proposed mechanism for the synthesis of the chloride salt.

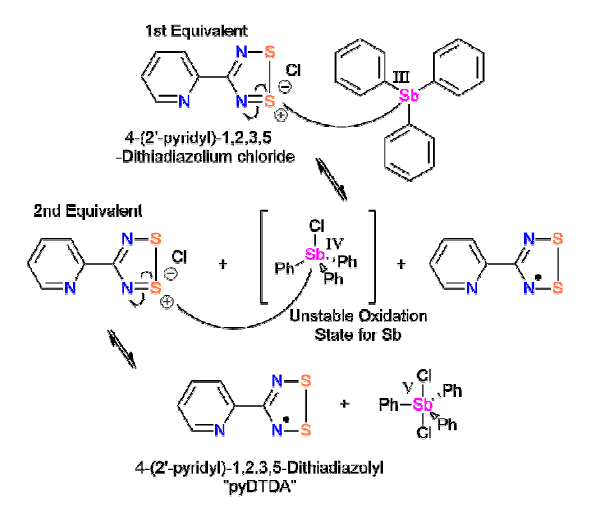


Figure 7. Starting from the chloride salt, shows the proposed mechanism for the synthesis of the pyridyl DTDA radical.

DTDA is a five-membered, planar ring with  $7\pi$  electrons that are resonance stabilized. The singularly-occupied molecular orbital (Figure 8) or SOMO for this moiety is located in a  $\pi^*$  (pi-antibonding) orbital, and its contributions are from the two sulphurs and two nitrogens (there is a node that goes through the carbon atom, preventing it from contributing to the SOMO). Since there is a node going through the carbon atom, it cannot make an irreversible sigma bond to another nearby DTDA heterocycle (such that the paramagnetic ligand would then become diamagnetic).

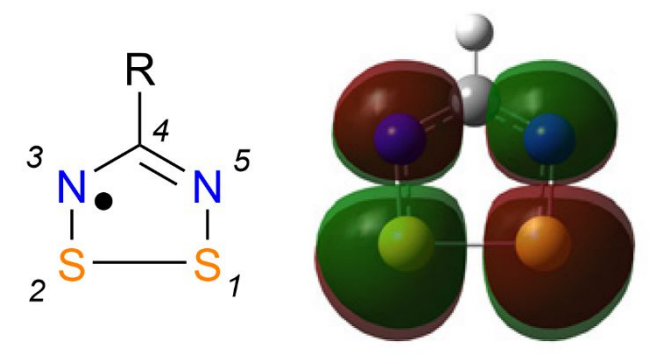


Figure 8. The 1,2,3,5-dithiadiazolyl moiety (DTDA) showing the distribution for the SOMO, where there is a node that goes through the carbon atom. DFT calculations (not this work) performed using B<sub>3</sub>LYP and a 6-3<sub>1</sub>G(d,p) basis set. See reference 8.

Although the carbon cannot directly cause or contribute to dimerization, there is a well-established phenomenon called pancake bonding or pi-stacking that can result in dimerization (read: diamagnetic ligand) for DTDA radicals.<sup>13</sup> Pancake bonding for DTDA has several orientations depending on the R group<sup>7</sup> (see Figure 9), but the most common is the cis-cofacial bonding mode. Upon dimerization, the intermolecular distance for planar paramagnetic species is usually less than the sum of the van der waals radii (2.8-3.3Å).

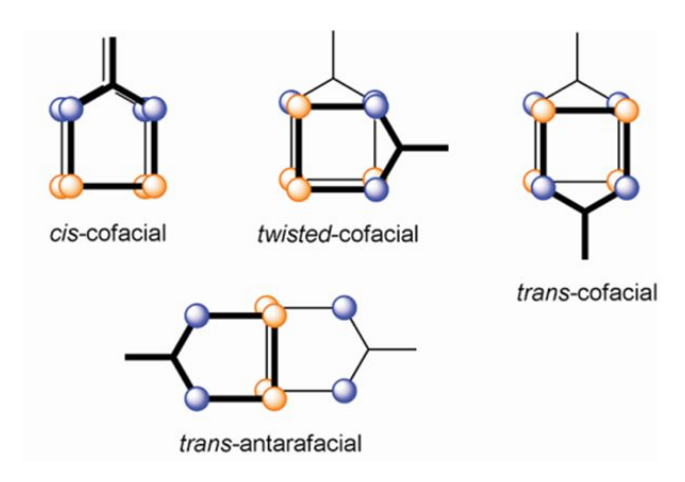


Figure 9. Pancake bonding modes for DTDA moieties, where proper orbital overlap, intermolecular distances, and orientation are required.<sup>7</sup>

The important difference between pancake bonding and regular sigma bonding is that pancake bonds are reversible.<sup>13</sup> Hence, for some species such as the transition metal complex Mn(II)(hfac)<sub>2</sub>pyDTDA (Figure 10), there exists a monomer-dimer equilibrium that is thought to be influenced by the temperature of the solution.<sup>14</sup> Note: hfac is the hexafluoroacetylacetonato ligand (see later discussion). The dimerization that occurs between metal-radical complexes is a hindrance to conductivity (in that the radicals from neighbouring paramagnetic ligands form an electron pair and cannot facilitate charge transfer) and magnetism (the ligand can no longer facilitate magnetic coupling between the metal centres).

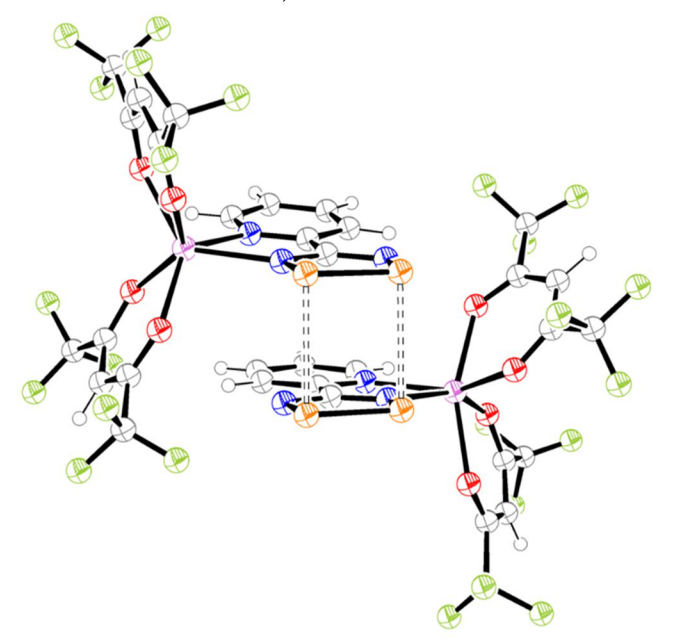


Figure 10. The crystal structure for Mn(II)(hfac)<sub>2</sub>pyDTDA from reference 14 that exists as a dimer in the solid state, where hfac is 1,1,1,5,5,5-hexafluoroacetylacetonato-. The closest intermolecular contacts (dotted lines) are 3.043 and 2.995Å.

Typical transition metal-radical complexes found in the Preuss group appear as in Figure 10. Other metals that have been used include Ni(II)15, high-spin Fe(II)15, Co(II)16, and Cu(II)<sup>14</sup>. The pyDTDA versions of these metal-radical complexes are dimerized in the solid state for Mn(II) and Cu(II), but not for Co(II), Ni(II), or Fe(II). The iron pyDTDA complex, however, is unstable and undergoes thermal decomposition.<sup>15</sup> For metal-radical complexes, the hfac ligand has two main purposes: (1) the fluorines are electron withdrawing groups that cause the metal centre to become a hard lewis acid, thus facilitating hard-hard interactions between the metal and the bidentate nitrogen pocket that is found in the boaDTDA and pyDTDA radicals. The hard metal is therefore less likely to form interactions with the sulphur groups of the DTDA heterocycle. (2) The fluorines are non-polarizable and do not exhibit strong F-F interactions. The London dispersion intermolecular forces are a lot lower for hfac than its hydrogen equivalent acetylacetonate (acac), which provides the metal-radical complexes with properties such as solubility and volatility. These properties are important for the sublimation technique that is used to purify and generate crystals for metalradical complexes.

The main goal of this project is to explore the possibility of generating a metal-radical complex with both conductive and magnetic properties, and to see how these properties interact. Since pancake bonding can cause serious issues for both of these aspects, a way to prevent the dimerization is henceforth discussed.

Similar to the Jahn-Teller distortion<sup>17</sup>, a Peierls distortion is an energy gain that results from a reduction in symmetry (removal of degenerate states). The cause of a Peierls distortion is that a 1D chain of equally spaced, half-filled constituents is unstable. Robert Haddon originally predicted that organic radical species could conduct like metals (for example sodium, which has one valence electron). Instead, these radicals undergo Peierls distortion and dimerize, similar to the pancake bonding that is observed for metalradical complexes. The most basic example of Peierls distortion occurs with hydrogen atoms (Figure 11). Hydrogen exists as a dimer, because there is an energy gain from dimerization.

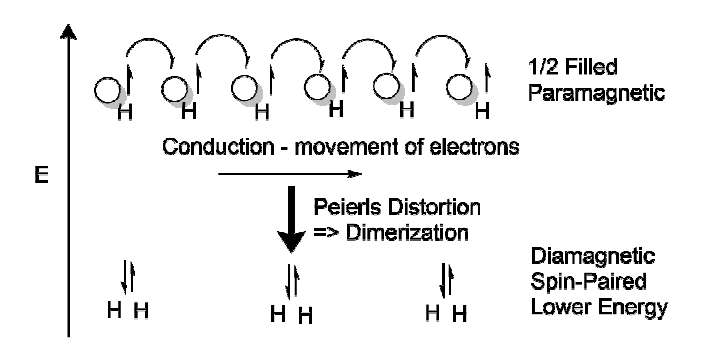


Figure 11. The Peierls distortion causes hydrogen to become a dimer, and could explain why some DTDA moieties undergo

pancake bonding. The basis of this distortion is that a 1D chain of equally-spaced, half-filled constituents is unstable.

In the solid state, the distribution of orbital energies for a given compound can be thought of as a band, where we have the lower conducting band and the higher valence band (Figure 12). For a metal, the valence band is partially full and allows for electrons to move freely and facilitate conductivity. For a semi-conductor, there is a small energy gap (band gap) of 0.5-3eV (electron volts). Under the application or possession of thermal energy, the electrons in the conduction band of a semi-conductor can be promoted to the conduction band to facilitate conductance. Lastly, an insulator has a large band gap (~6eV), and few electrons have enough thermal energy to be promoted to the conductance band.

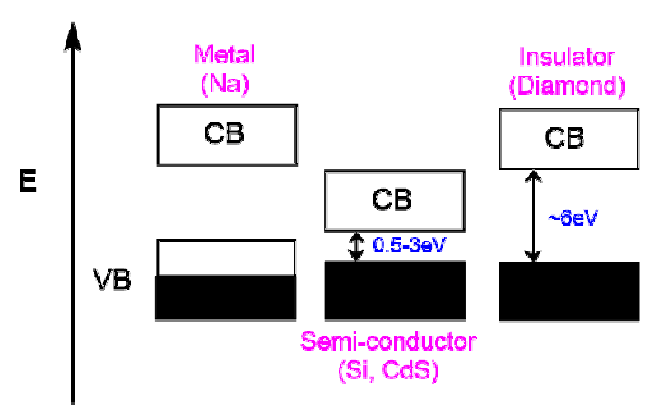


Figure 12. Band theory for metals, semi-conductors, and insulators with example materials and applicable band gaps shown. CB = conductance band, VB = valence band.

Doping can also be explained using band theory, and the two types are n-dopants and p-dopants (Figure 13). An n-dopant becomes oxidized and reduces a material, generating a higher population of electrons in the conductance band. A p-dopant becomes reduced and oxidizes a material such that electron holes form in the valence band. Notice that a p-doped semi-conductor has a similar appearance to the band structure of a metal as in Figure 12.

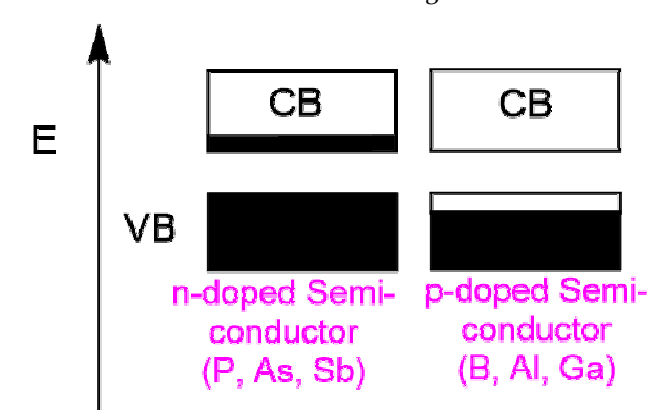


Figure 13. Band theory for n- and p- type dopants with examples shown. CB = conductance band, VB = valence band.

Band theory can also be used to help explain a Peierls distortion and how it might be prevented (Figure 14). Using a p-dopant for the radical species might prevent a Peierls distortion by lessening the energy gain from dimerization. A charge density wave (CDW) is the periodic modulation of charge density in a crystal lattice that is caused by the distribution of electrons. The CDW can be approximated by the equation:

$$y = Asin(q2\pi n + p)$$

Where A is the amplitude of the sine wave, q is the electron filling, n is the integer value representing the radical, and p is the phase shift.

The impact of dimerization, where the electron filling is 1/2, can be seem in the CDW in Figure 14. Upon doping, the CDW will change as the distribution of the radicals is no longer uniform. For example, if we use a p-dopant such that the filling is less than 1/2 - 1/4 or 3/8 – full, the CDW looks more like in Figure 15.

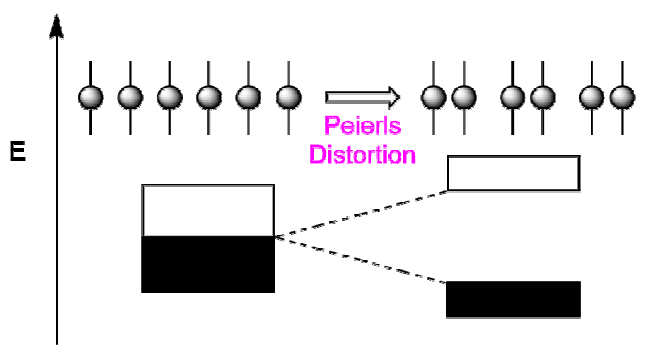


Figure 14. A band theory representation of a Peierls distortion. The leftmost part of the figure shows a 1D chain of radicals, which dimerize as per the right-hand side to give a band gap. The radicals can also be thought of as components of a charge density wave, explained in the text.

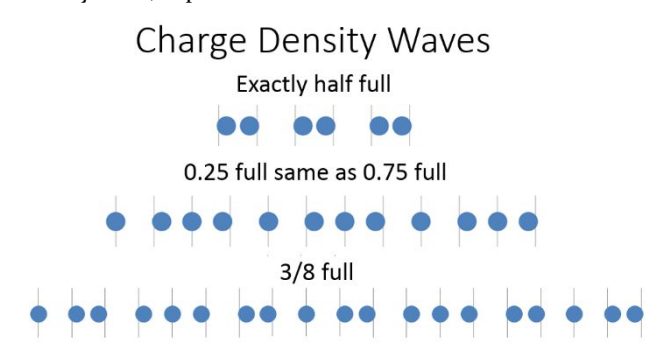


Figure 15. Charge density waves (CDW) can be used to explain the distribution of electrons in a lattice. The top CDW is for a valence band that is exactly half full, and there is a dimerization that occurs as seen with Peierls distortion. With filling that is no longer 1/2, the modulation of the lattice with respect to charge density changes. The 1/4 filling appears as a 1:3:1 repeat, and the 3/8 filling appears as a 1:2:3:2:1 repeat.

Materials exhibit changes in conductivity differently depending on their band structure. Conductivity ( $\sigma$ ) is described by the equation:

$$\sigma = n|e|\mu$$

Where n is the number of charge carriers, e is the charge of the electron in coulombs (1.602x10<sup>-19</sup>C), and  $\mu$  is the mobility of the charge carriers.<sup>19</sup> For a metal, the number of charge carriers is high, and the limiting factor for conductivity is the charge mobility. The mobility for charge carriers in metals decreases with increasing temperature, because the number of electron-phonon collisions increases (thus reducing charge mobility). For a semi-conductor, the number of charge carriers is the limiting factor for conductivity. The number of charge carriers increases with increasing temperature, due to the promotion from the valence to the conduction band. Another way to increase the conductivity for a semi-conductor is to use dopants (which can also be referred to as impurities) that either provide electrons or holes (Figure 13). In the case where the temperature of a semi-conductor is increased, the number of charge carriers (n) can be described by:

$$n = \frac{n_0}{e^{\frac{E}{k_B T}}}$$

Where  $n_o$  is the total number of electrons, E is the activation energy in electron volts needed to promote an electron to the conduction band,  $k_B$  is the Boltzmann constant, and T is the temperature in Kelvin. Note the "e" here refers to the irrational number and not the elementary charge. In increasing the temperature of a semi-conductor, the relationship is that the number of charge carriers, and thus the conductance, increases with increasing temperature.

The behaviour of an insulator with respect to temperature is the same as a semi-conductor, except the magnitude of conductivity is much lower. Since the band gap for an insulator is much larger than for a semi-conductor, the value for E is larger and the value for n is relatively smaller (resulting in lower conductivity). Typical conductivity values are 10³-106 Siemens/cm for metals, 10°3-102 Siemens/cm for semi-conductors, and less than 10°7 Siemens/cm for insulators.

Organic compounds are generally not thought of as good conductors; however, a class of conductive organic compounds are known and these compounds are called charge transfer (CT) salts. The first example of an organic metal – that is, a compound whose conductivity decreased with increasing temperature - was tetrathiofulvalene (TTF) and tetracyano-p-quinodimethane (TCNQ) as shown in Figure 16.20 For long-range conduction, the important factor is thought to be the separate, alternating stacks. 19 TTF is a pielectron donor, whereas TCNQ is a pi-electron acceptor. The donor stacks seen in Figure 16 are capable of transferring some charge to the acceptor stacks, which produces a partially occupied, pi electron band. 19 Since this is a partial charge transfer, the compounds are not exactly half-filled and do not dimerize, as seen by the equal spacing between the constituents.

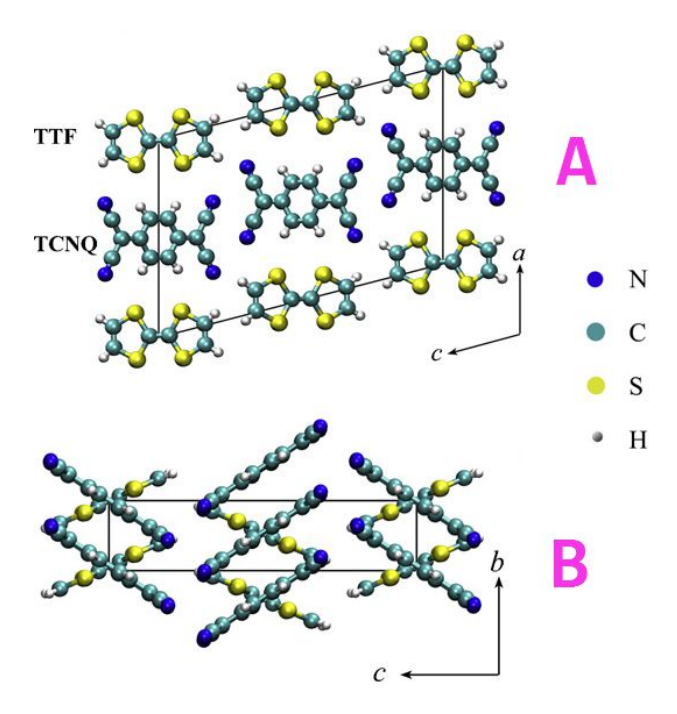


Figure 16. The crystal structure of TTF-TCNQ (image taken from reference 21). Image A shows the orthogonal view along the stacking b-axis, and image B shows the orthogonal view along the direction at right angles to the (bc)-plane of TTF-TCNQ. The space group for this structure is  $P2_1/C$ . <sup>21</sup>

In order to procure conductivity in DTDA radical species and metal-radical complexes, the proposed method is by using a dopant to facilitate partial charge transfer. This method was used successfully in Oakley's group for the 1,4phenylene-bis(dithiadiazolyl) diradical as seen in Figure 17, where iodine is used as a p-dopant to prevent dimerization and facilitate charge transfer.<sup>22</sup> This compound shows semi-conductor behaviour below 200K, as its conductivity increases with increasing pressure.22 From 210K until decomposition, the compound exhibits weak metallic conductivity.22 The highest conductivity for this compound was 100 Siemens/cm at 350K, and under the application of pressure (1.5GPa) the conductivity increases by a factor of approximately 4.22 This increasing conductivity with increasing pressure is known in other metallic species such as hydrogen.

The phenyl DTDA (phDTDA) radical was also doped with iodine, as seen in Figure 18.<sup>23</sup> However, this compound forms the triple-decker salt [phDTDA]<sub>3</sub>+[I<sub>3</sub>]-, where each phDTDA has a charge of 1/3+.<sup>23</sup> The CDW for a 1/3 filled band shows groups of three, as in Figure 18, rather than the evenly spaced constituents that are desired for a charge-transfer salt. Synthesis of either the phDTDA and iodine, or diradical version with iodine, can be accomplished by co-subliming the species in an evacuated glass tube.<sup>22,23</sup>

This project involves the investigation of using iodine as a p-dopant for metal radical materials, as was accomplished with Oakley's group, to generate charge-transfer complexes. First, the materials must be screened to determine which ones are suitable for doping. Previous charge transfer salts rely on the reversibility of oxidation and reduction states between the compounds involved as to facilitate charge transfer. Therefore, the metal-radical complexes must also be able to undergo reversible redox processes to enable conductance.

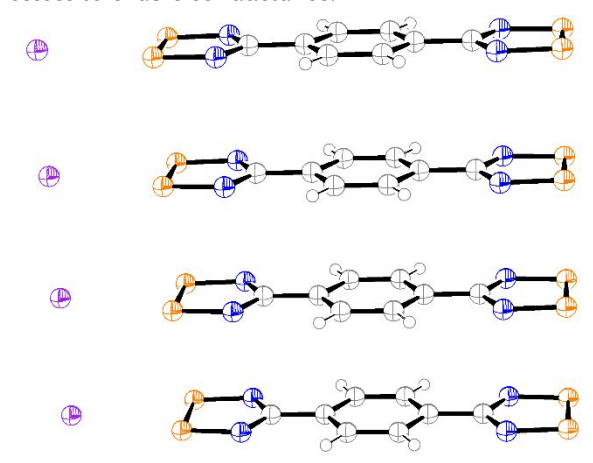


Figure 17. Crystal structure for 1,4-phenylene-bis(dithiadia-zolyl) diradical when doped with iodine in a 1:1 molar ratio. Notice the even spacing means that the radicals did not undergo dimerization. Iodine (purple), nitrogen (blue), sulphur (orange), carbon (white), and hydrogen (small white).

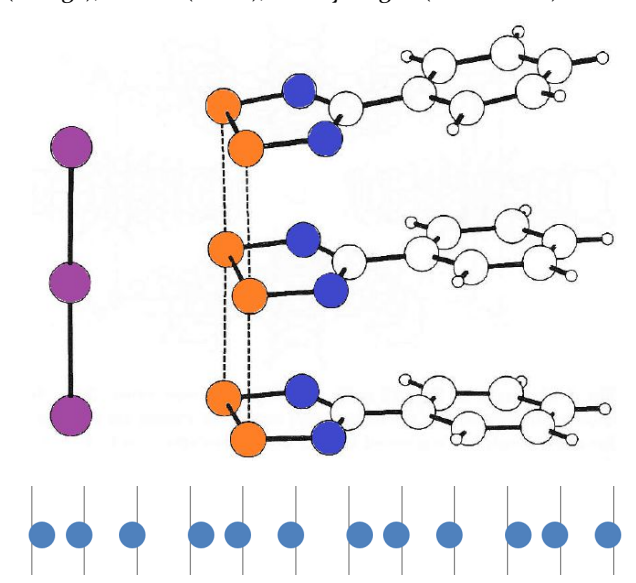


Figure 18. The crystal structure for  $[phDTDA]_3[I]_3$  – Top- with the same colour scheme as in Figure 17, and – Bottom- CDW as predicted using the formula with a q value of 1/3.

The metals mentioned for pyDTDA complexes (Fe(II)-hs, Ni(II), Mn(II), Cu(II), Co(II)) have been tested for their redox processes previously in the Preuss group using cyclic voltammetry (CV). Of these metals, Ni(II), Mn(II), and Co(II) show potentially reversible oxidative processes. Last semester, the student synthesized the metal starting materials (M(hfac)<sub>2</sub>(THF)<sub>2</sub>, where M = Ni, Mn, Co), according to

Scheme 2. The synthesis of the metal-radical complex from the metal precursor and the radical is discussed in references 14, 15, and 16.

Scheme 2. The overall synthesis for a metal precursor for metal-radical complexes. First, the metal is coordinated to hfac (hexafluoroacetonato) in an aqueous environment, followed by a reaction in dry solvent and coordination to tetrahydrofuran (THF).

The CV data for Ni(II) is shown in Figure 19, and the crystal structure for this complex (Ni(hfac)<sub>2</sub>pyDTDA) is shown in Figure 20. Looking at the red curve (applied oxidative potential), when the complex loses electrons, there is a peak at 1.36V. Upon the re-reduction process, there is a peak at 1.01V. Since these peaks do not occur at the same potentials, this process is not electrochemically reversible (difference of 350mV). However, the peak areas are approximately equal, and so the process is likely chemically reversible. It also means that the complex does not compose under oxidation, which is important if the complex is to facilitate charge transfer with iodine.

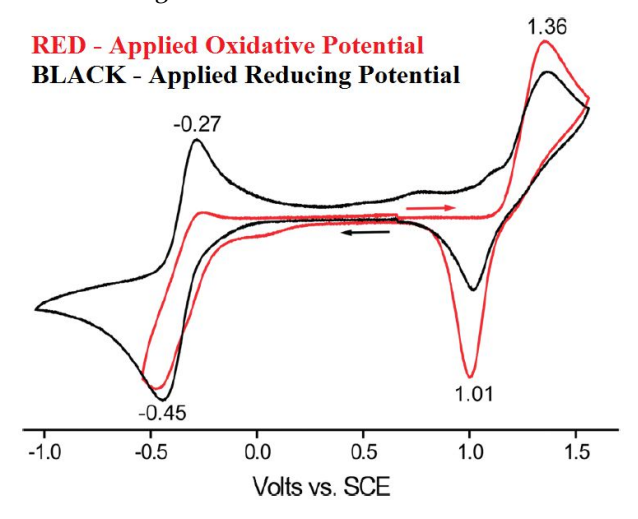


Figure 19. CV data for Ni(hfac)<sub>2</sub>pyDTDA complex from reference 15. Measurements were performed at room temperature in  $CH_2Cl_2$  using 0.05M  $nBu_4NPF_6$  as a supporting electrolyte, with a scanning rate of 0.5 Volts/second.

Since there are metals and radicals present in the complex, the redox properties of the metal precursors (M(hfac)<sub>2</sub>(THF)<sub>2</sub>) were also tested using CV to see whether the metal or the radical is likely to be affected by redox processes as part of a complex. For the Ni metal precursor, no redox processes were observed in the solvent window under similar conditions as run for the metal-complex.<sup>15</sup> This observation makes chemical sense, as Ni(II) is a stable oxidation state, and fewer Ni compounds are seen with oxidation state I or III. Furthermore, this result implies that the oxidation process observed in Figure 19 is an oxidation of the radical species from [pyDTDA]• to [pyDTDA]+.



Figure 20. Crystal structure for the Ni(hfac)<sub>2</sub>pyDTDA complex. Fluorine (pink), nitrogen (blue), sulphur (orange), nickel (green), oxygen (red), carbon (grey), hydrogen (small grey).

The cobalt complex<sup>14</sup> is similar to the nickel complex, in that there is a chemically reversible, yet electrochemically irreversible, oxidation process (Figure 21). The cobalt metal precursor also does not show any redox processes in the range -1.5-2.oV; therefore, the complex does not decompose under oxidation and most likely changes from [Co<sup>1-</sup>DTDA•] to [Co<sup>11</sup>DTDA+]+.<sup>14</sup>

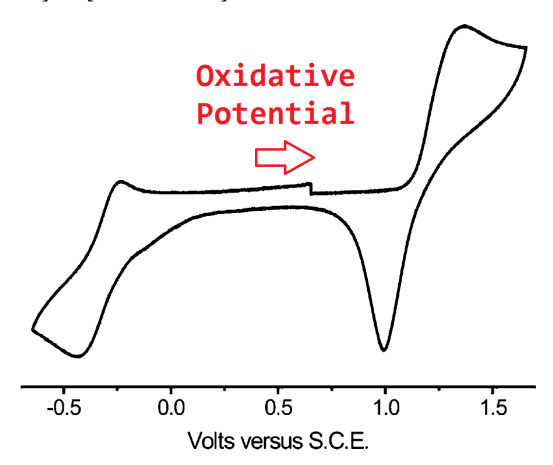


Figure 21. CV data for Co(hfac)<sub>2</sub>pyDTDA from reference 14. Measurements performed as in Figure 19.

The manganese complex is somewhat more complicated with regards to CV data (Figure 22). For Figure 22a, the oxidative sweep is limited to 1.50V, and a chemically reversible oxidation is seen as with the Ni and Co complexes. This CV shows that [Mn<sup>II</sup>DTDA+] is oxidized to [Mn<sup>II</sup>DTDA+]+ without decomposition. For Figure 22b, the oxidative sweep is extended to 2.50V, and three peaks are seen. The first one-electron oxidative peak is a result of the DTDA, and the second one-electron oxidative peak is the oxidation of the manganese from Mn(II) to Mn(III). However, the [Mn<sup>III</sup>DTDA+]2+ species likely undergoes a rearrangement to the more stable [MnIVDTDA•]2+ complex. The third peak, on the returning reduction sweep, is approximately the area of the first two oxidative peaks combined. Thus, it is likely the two-electron reduction back to the original neutral complex [Mn<sup>II</sup>DTDA•]. No decomposition is observed for this compound.14

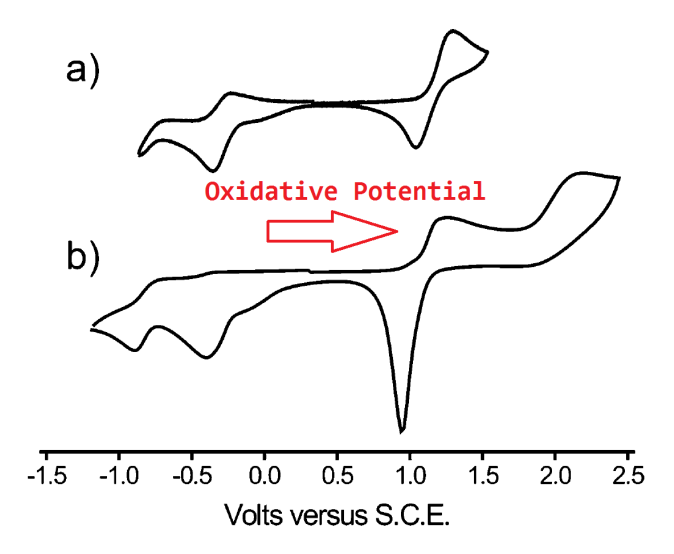


Figure 22. CV data for Mn(hfac)<sub>2</sub>pyDTDA from reference 14. Measurements performed as in Figure 19. Part a shows the oxidative sweep in the range -0.85-1.50V, and part b shows the oxidative sweep in the range -1.25-2.50V.

The last piece for explanation as a precursor for this project is the use of iodine as a dopant. Since previous work by Oakley has shown the successful use of iodine in making CT compounds with DTDA radical species, it is a good starting dopant to use with metal-radical complexes involving DTDA. Iodine can exist as I<sup>-</sup>, I<sub>3</sub><sup>-</sup>, and I<sub>2</sub>, and is also an easy compound to work with compared to other halogens. It is a solid at room temperature, and is easily purified through sublimation (Figure 23).

Rather than co-sublime iodine with the metal-radical complexes to afford doping, the project involves grinding the iodine with metal-radical complexes already available in the glove box using a mortar and pestle. This is a much faster technique that does not require a lot of material or skill with sublimation. Techniques for determination of successful doping include differential scanning calorimetry

(DSC) and powder x-ray diffraction (PXRD). For this project, the student used these two techniques to characterize radical starting materials and to observe the changes caused by adding iodine as a p-dopant.

An important aspect of the DSC technique is that it involves heating the sample. It is thought that the heating might be able to mimic the sublimation technique, and accounts for the need for heating if it is necessary for successful iodine doping. A brief discussion on DSC and PXRD theory is now given.

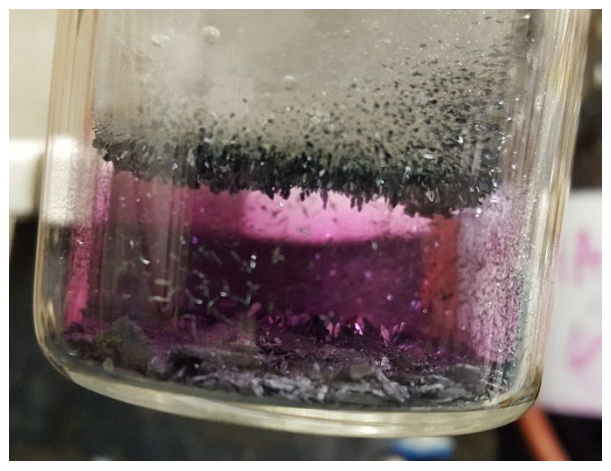


Figure 23. Iodine sublimation attached to the Schlenk line. Use of a heat gun enables the iodine to sublime and crystals form on the cold finger.

For PXRD, a filament in a cathode ray tube is heated to produce electrons. These electrons are accelerated towards a "target" (not the sample) by applying voltage (on the order of 30,000V) until the electrons have the energy necessary to eject inner shell electrons from the 1s level. Electrons in higher orbitals (i.e. 2p, 3p) immediately relax back to the 1s level, and emit photons with wavelengths on the order of 10-10 m (x-rays!).19 The target can be made of Cu, Fe, Mo, Cr, etc. The resulting x-rays from the target are wavelength specific depending on the sizes of the energy levels. For example, using Cu generates two main x-ray wavelengths of 1.5418Å and 1.3922Å, called K $\alpha$  and K $\beta$ , that represent the relaxation from the 2p -> 1s and 3p -> 1s energy levels respectively.19

PXRD can be compared to the diffraction of light by a grating, which is 1D whereas PXRD is a 3D process. A grating consists of evenly spaces grooves in a material (such as glass). As the light hits these grooves, it is diffracted at a certain angle relative to the groove angle. The combination of two diffracted wavelengths that are in phase causes constructive interference (wave grows larger). Conversely, two waves that are exactly out of phase will cancel one another out through constructive interference. Wavelengths that are not in or out of phase result in less intense diffracted beams

To get the PXRD diffractogram (*not* spectrum), the x-rays are collimated and directed at the sample. The intensity of the reflected x-rays from the sample is measured as

a function of incident angle. A peak is a result of constructive interference that occurs when the incident x-ray hits the sample and satisfies the Bragg equation. The Bragg equation is based on a model for how a crystal lattice diffracts light:

$$\frac{n}{\lambda} = 2dsin\theta$$

Where n is a positive integer,  $\lambda$  is the incident wavelength, d is the separation distance between the aligned planes of the lattice, and  $\theta$  is the incident angle.

PXRD is beneficial for this project in that it allows for the sampling of air-sensitive materials. The diffractogram is unique for each compound, as each crystal lattice refracts light uniquely. The analyte is carefully ground and poured into a capillary tube inside the glovebox. The capillary is temporarily sealed with vacuum grease until it is removed from the glovebox, after which the glass capillary is it flame-sealed. The quality of the PXRD diffractogram is determined by how well the sample packs in the capillary, and by the crystalline content of the material. The PXRD machine used for this project is depicted in Figure 24.



Figure 24. PXRD machine (nickname "Panda") used for sample measurement, set up with a spinning capillary tube in the centre for the sample. The right "arm" of the machine is capable of rotating to measure the diffracted x-rays for the angle range specified.

The student used PXRD from 4-40° to collect the spectra for starting materials. The idea here is to know what the individual components look like, such that the doped versions with iodine can be distinguished from an "admixture", or an overlap of both compounds, in the diffractogram. Instead, a new compound has hopefully formed, and new peaks are present in the diffractogram.

After performing PXRD of iodine, the student did not see any peaks for the diffractogram. A second PXRD attempt was made on a freshly sublimed/ground sample of iodine, but the results did not change. Since iodine was difficult to grind up, it may have packed poorly in the capillary. Instead, the PXRD was calculated (Figure 25) in the program *Mercury* using a single-crystal structure file (CIF) for I<sub>2</sub>, which the student downloaded from the Crystallography Open Database.<sup>24</sup> The student completed successful PXRD analysis on phDTDA (Figure 26), pyDTDA (Figure 27), and Ni(hfac)<sub>2</sub>pyDTDA (Figure 28). The same method was used

to measure the presented samples: scan step size 0.003283, 10967 sample points, with 18.87 as time per step, and a divergence slit of 0.10mm. An attempt to measure previously co-sublimed iodine and phDTDA was made, but this diffractogram was very poor and had a high noise content (Figure 29).

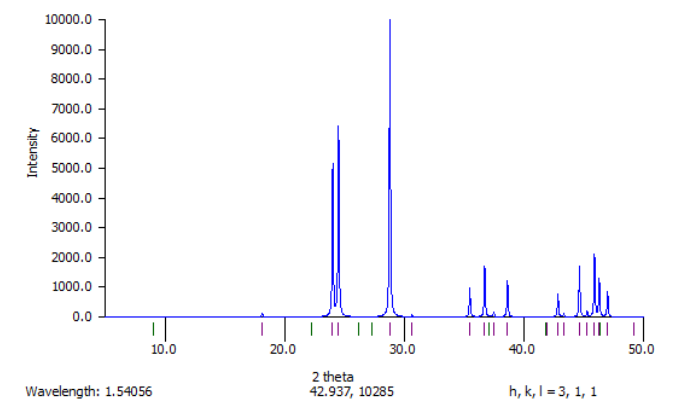


Figure 25. Calculated PXRD diffractogram for iodine (I<sub>2</sub>). Program used was Mercury. Original paper for crystal structure is reference 24.

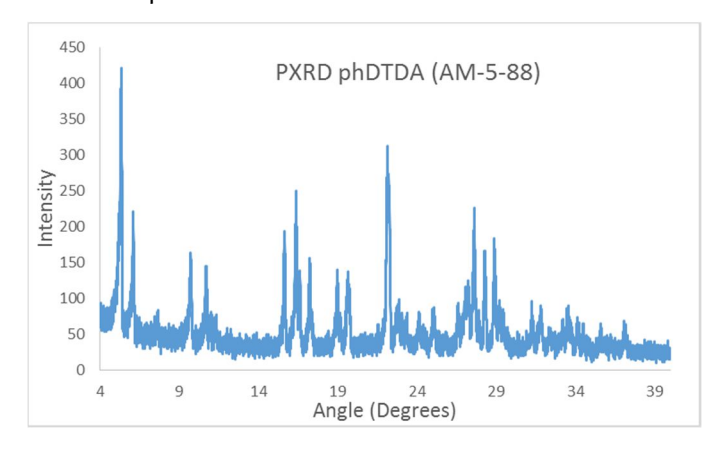


Figure 26. Diffractogram for phDTDA radical from AM-5-88.

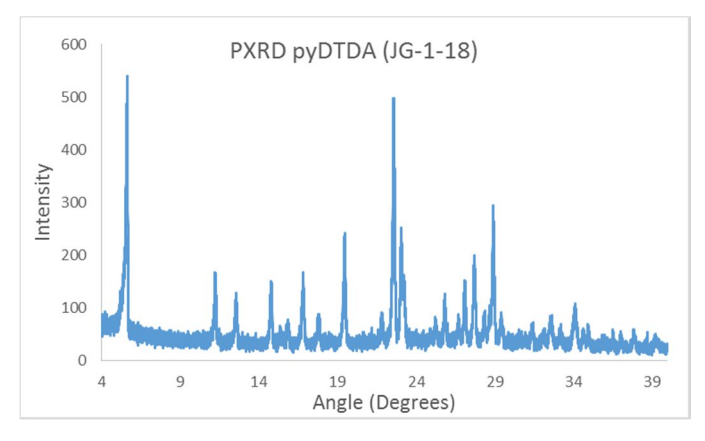


Figure 27. Diffractogram from student's sample of pyDTDA radical (JG-1-18).

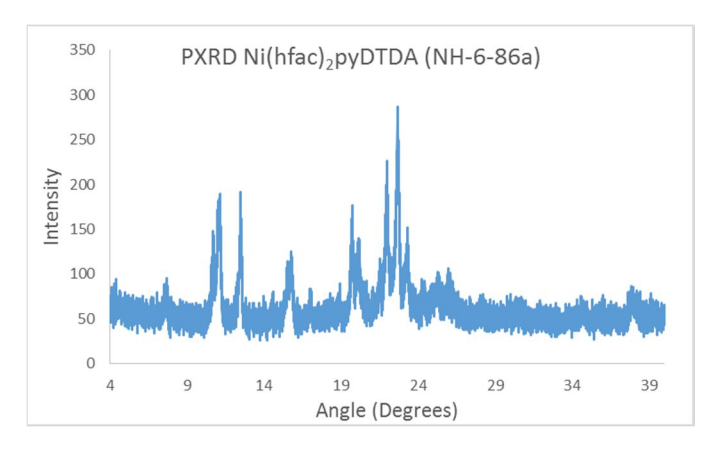


Figure 28. Diffractogram for Ni(hfac)<sub>2</sub>pyDTDA complex from NH-6-86a. Note first sample decomposed (was exposed to air), and so this is a repeat.

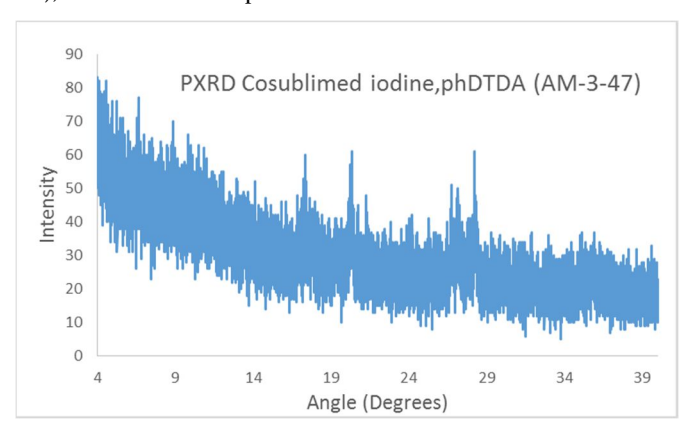


Figure 29. Attempted diffractogram for cosublimed iodine and phDTDA sample from AM-3-47. Possible explanations for the poor results are improperly ground sample, decomposed sample, improper use of equipment (filters, alignment, etc.), and poor packing.

Next, the methodology and use for determining successful doping for DSC will be discussed. DSC works by simultaneously heating a sample pan and a reference pan. The heat flow needed raise (or lower) the temperature of the sample pan relative to the reference is measured as a function of changing temperature. For crystalline materials, two types of peaks are usually observed representing phase changes for the compound, where a peak pointing down is an endothermic process (melting, sublimation, evaporation) that requires energy and a peak pointing up is an exothermic process (recrystallization, condensation) that gives off energy relative to the empty pan.

DSC can also be catered to air-sensitive materials, such that a T-zero hermetically sealed pan (Figure 30) can be pressed to contain the sample inside of the glovebox. The sample can then be measured without exposure to air. Only 2-5mg of sample is needed for measurement, and so large scale synthesis is not required for thermal characterization. The instrument is shown in Figure 31.





Figure 30. T-zero aluminium hermetically-sealed pan (left) and lid (right) for DSC measurement of air-sensitive materials.



Figure 31. DSC Q2000 TA Instrument as used for thermal analysis of iodine-doped radicals and metal-radical complex. Picture from Professor Dmitriy Soldatov's website.

Reference pans for this work were pressed inside the glovebox. All heating and cooling cycles were performed at a rate of 5°C/minute. The DSC of iodine was performed by the student (Figure 32). This experiment was repeated multiple times in an attempt to discern the cause of the exothermic peaks around the melting point of iodine (113°C). The expected thermogram should show a melting peak (endotherm – pointing down) at ~114°C, and a sublimation/evaporation peak (endotherm – pointing down) at ~184°C. It is now thought that the iodine is reacting with the aluminium sample pan to cause the weird exothermic peaks, and so the DSC measurement for iodine could be conducted in copper, gold, graphite or alumina instead as a reference (with note that only Cu pans can be hermetically sealed).

The student also performed DSC measurements of compounds according to Table 1 below. Note all samples were ground prior to analysis. Iodine was ground in a 1:1 molar ratio where indicated. Unless otherwise specified, samples where heated and cooled for three cycles, starting with a cool to -85°C followed by a heating phase to 230°C at 5°C/min.

Table 1. DSC experiments as completed by the student. Key: m.p. = melting point (endotherm), subl. = sublimation (endotherm), cryst. = crystallization (exotherm). Peak maxima are given for the first heating cycle of each compound.

Compound	Notes (1st heating cycle)
Iodine	m.p 113°C, subl. 189°C
Both as I <sub>2</sub> sublimed single crystal and ground sample	
pyDTDA AM-5-88	subl. 118°C
phDTDA JG-1-18	3 subl. 109, 127, 130°C
[I][phDTDA] ground	subl. 170°C, cryst. 183°C
[I][pyDTDA] ground	2 subl. 168, 171°C, cryst. 191°C
Ni(hfac)₂pyDTDA	subl. 188°C
NH-6-86a	
[I][Ni(hfac)₂pyDTDA] ground	subl. 192°C, subsequent start of cryst.

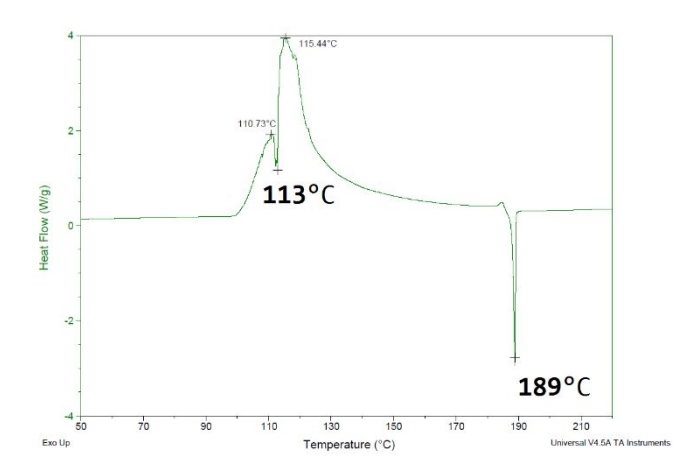


Figure 32. Thermal profile for iodine upon heating to 230°C from -85°C. The exotherms surrounding the melting point are thought to be a result of reaction with the aluminium pan.

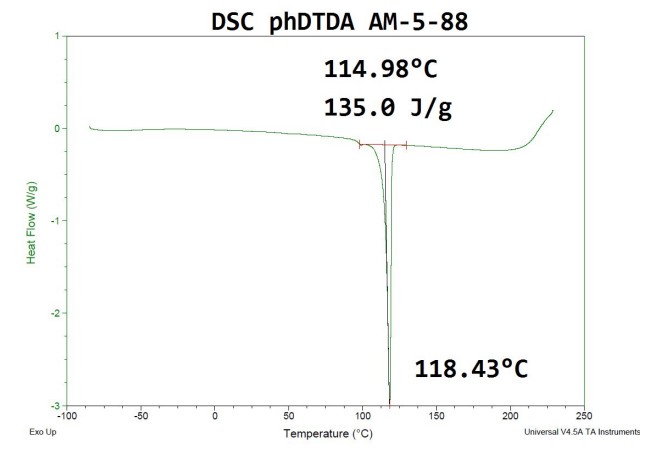


Figure 33. Example heating profile for phDTDA radical.

The DSC plots themselves do not afford great insight unless scrutinized, and so a discussion will be made here instead of trying to show the various heating and cooling events in detail. Starting with the radical species, phDTDA and pyDTDA, these compounds exhibited sublimation points at 118°C for phDTDA and 109, 127, and 130°C for pyDTDA. The triple peak for pyDTDA may indicate the presence of impurities in the sample; this phenomena was repeatable for three separate runs of the same compound. Upon cooling, the radicals exhibited "supercooled" peaks (which appear as loops in the DSC plot). These indicate that the compound did not manage to reform as a solid. The student attempted to reform the solid by allowing the sample to sit at o°C for 1hr in between cycles, but this did not improve the results. However, for one sample that was lower in mass (1.5mg), a proper recrystallization peak was observed (pyDTDA 62°C exotherm). The fact that the samples are under pressure is therefore thought to contribute to the sample's inability to reform completely as a solid.

The next samples that were analyzed involve grinding iodine as a 1:1 molar ratio with pyDTDA and phDTDA in the glove box using a mortar and pestle. These samples did not show sublimation points at the temperatures of the radical starting materials. Nor did the melting point of iodine appear in these plots. Instead, the observed sublimation peaks (endotherms) were at higher temperatures for the materials that were ground with iodine. Specifically, on the heating cycle for phDTDA and iodine, an endotherm was observed at 170°C. On the heating cycle for pyDTDA and iodine, two endotherms were seem at 168°C and 171°C, which is approximately the temperature difference (3°C) seen for two of the sublimation peaks of the radical. For the first heating cycle, the radical/iodine ground samples exhibit a wide exotherm following the sublimation peaks. Interestingly, for all samples ground with iodine, no form of recrystallization or sublimation peaks were present in the DSC following the first heating cycle. This lack of data is taken to mean that a new compound has formed, and reguires a higher temperature in order for a subsequent melting/sublimation peak to be observed.

For the Ni(hfac)<sub>2</sub>pyDTDA complex, this compound has a sublimation peak that is very close to the sublimation of iodine. This factor might make it difficult to separate the two in a combined sample. However, the ground metal-radical complex with iodine shows similar behaviour to the radical and iodine ground sample. There is an endotherm for sublimation, followed by the start of a wide exotherm, and finally no other peaks are seen in subsequent heating and cooling cycles. This sample should be heated to a higher temperature to see if another, iodine-doped compound has been made with a distinct thermal profile.

Other work that was attempted by the student was to reproduce a thermogram for a cosublimed iodine and phDTDA sample (made by a previous student). However, the only evidence that this compound was successfully synthesized was IR, and PXRD did not show any helpful information. The student decided that this compound was

not suitable as a reference and may have decomposed or altered composition/structure/crystallinity since it was made.

In conclusion, the work for the project of using iodine as a dopant for metal-radical materials has been outlined, and the current progress with regards to characterizing the materials using DSC and PXRD has been explained. Since the radical and metal-radical complex that were tested show different thermal profiles under DSC than their starting materials, the next step should be to synthesize more Ni(hfac)<sub>2</sub>pyDTDA complex and co-sublime with iodine. The conductivity of this sample could then be measured to see if successful doping and prevention of Peierls distortion has occurred.

Future work should also be to characterize the metalradical complexes for manganese and cobalt, as well as for the boaDTDA radical.

Over this two-semester project, the student has been able to learn the synthesis of DTDA radicals and metal precursors. Also, the techniques for PXRD and DSC have been employed by the student to some measurable amount of success.

One concern for this work is the sample size; since mg quantities were used for the preparation of the ground samples with iodine, the error with regards to molar ratio is high. Future work should be directed to make larger quantities of these ground materials, and to try and distinguish the difference between using different amounts of iodine (for instance, what happens when 4 equivalents of iodine is added instead of 1?).

If crystalline samples of the doped Ni-py species are obtained, the PXRD diffractograms have been made available by the student for direct comparison to see whether a new compound has formed (rather than a simple admixture).

### **AUTHOR INFORMATION**

### **Corresponding Author**

\* jgarneoı@mail.uoguelph.ca

### Notes

This paper is to be submitted to Professors Kathryn Preuss and Professor William Tam at the University of Guelph for the CHEM\*4910 course (Undergraduate Research Project).

### **ACKNOWLEDGMENT**

I would like to thank my supervisor Professor Kathryn Preuss for allowing me to work in her laboratory on this project, and also for her help in explaining the concepts behind the work at group meetings and during practice talks. I would also like to thank Danielle Dinsdale, who helped me to run the PXRD on my samples, as well as for her help in running my experiments. Thanks for Adam Maahs for his shared material for background information, as well as his help for generating images for crystal structures. Thank you to the rest of the Preuss group: Parnian Soltanipanah, Keira Page-Davis, Tobie Wohlhauser, Robert (Alex) Mayo, Saleh Faleh Alofi, and Michelle

Mills. Thank you to Professor Dmitriy Soldatov for allowing me to use his DSC machine, and to his group members who assisted me with its use: Laszlo Visontai, Eliza Poloz, Farukh Ali, Andrew Tsang, and Mohamed Ghazzali. Finally thank you to Professors Richard Manderville and William Tam for their support in grading my talk and paper respectively.

### **REFERENCES**

- (1) Caneschi, A.; Gatteschi, D.; Sessoli, R.; Rey, P. Toward Molecular Magnets: The Metal-Radical Approach. *Acc. Chem. Res.* **1989**, 22, 392-398.
- (2) Gupta, K.B.S.S.; Alia, A.; de Groot, H.J.M.; Matysik, J. Symmetry Break of a Special Pair: Photochemically Induced Dynamic Nuclear Polarization NMR Confirms Control by Nonaromatic Substituents. *J. Am. Chem. Soc.* **2013**, *13*5, 10382-10387.
- (3) Denmark, S.E. Catalysts break symmetry. *Nature*, **2006**, *443*, 40-41.
- (4) Karakaya, I.; Karabuga, S.; Mart, M.; Altundas, R.; Ulukanli, S. Synthesis and Catalytic Asymmetric Applications of Quinazolinol Ligands. *Synthesis*, **2016**, *48*, 1719-1726.
- (5) Alaria, J.; Borisov, P.; Dyer, M.S.; Manning, T.D.; Lepadatu, S.; Cain, M.G.; Mishina, E.D.; Sherstyuk, N.E.; Ilyin, N.A.; Hadermann, J.; Lederman, D.; Claridge, J.B.; Rosseinsky, M.J. Engineered spatial inversion symmetry breaking in an oxide heterostructure built from isosymmetric room-temperature magnetically ordered components. *Chem. Sci.* 2014, 5, 1599-1610.
- (6) Sheridan, U.; Gallagher, J.F.; McGinley, J. Synthesis and structural studies of new asymmetric pyridyl-tetrazole ligands for supramolecular chemistry. *Tetrahedron*. **2016**, 72, 8470-8478.
- (7) Preuss, K.E. Metal complexes of thiazyl radicals. *Dalton Trans.* **2007**, 23, 2357-2369.
- (8) Preuss, K.E. Metal-radical coordination complexes of thiazyl and selenazyl ligands. Coordin. Chem. Rev. **2015**, *289-290*, 49-61.
- (9) Felthouse, T.R.; Dong, T.Y.; Hendrickson, D.N.; Shieh, H.S.; Thompson, M.R. Magnetic Exchange Interactions in Nitroxyl Biradicals Bridged by Metal-Metal Bonded Complexes: Structural, Magnetochemical, and Electronic Spectral Characterization of Tetrakis(perfluorocarboxylato)dimetal(II) Complexes of Rhodium and Molybdenum Containing Axially Coordinated Nitroxyl Radicals. *J. Am. Chem. Soc.* 1986, 108, 8201-8214.
- (10) Eaton, G.R. EPR Studies of Metal Complexes Containing Nitroxyl Radicals. *Inorg. Nucl. Chem. Letters.* **1972**, *8*, 647-652.
- (11) de Nooy, A.E.J.; Besemer, A.C.; van Bekkum, H. On the Use of Stable Organic Nitroxyl Radicals for the Oxidation of Primary and Secondary Alcohols. *Synthesis*, **1996**, *10*, 1153-1176.
- (12) Sheldon, R.A.; Arends, I.W.C.E. Organocatalytic Oxidations Mediated by Nitroxyl Radicals. *Adv. Synth. Catal.* **2004**, *346*, 1051-1071.
- (13) Preuss, K.E. Pancake bonds: pi-Stacked dimers of organic and light-atom radicals. *Polyhedron*, **2014**, *79*, 1-15.
- (14) Britten, J. Hearns, N.G.R.; Preuss, K.E.; Richardson, J.F.; Bin-Salamon, S. Mn(II) and Cu(II) Complexes of a Dithiadiazolyl Radical Ligand: Monomer/Dimer Equilibria in Solution. *Inorg. Chem.* **2007**, *46*, 3934-3945.
- (15) Hearns, N.G.R.; Fatila, E.M.; Clerac, R.; Jennings, M.; Preuss, K.E. Ni(II) and *hs*-Fe(II) Complexes of a Paramagnetic Thiazyl Ligand, and Decomposition Products of the Iron Complex, Including an Fe(III) Tetramer. *Inorg. Chem.* **2008**, *47*, 10330-10341.
- (16) Hearns, N.G.R.; Preuss, K.E.; Richardson, J.F.; Bin-Salamon, S. Design and Synthesis of a 4-(2'-Pyridyl)-1,2,3,5-Dithiadiazolyl Cobalt Complex. *J. Am. Chem. Soc.* **2004**, *126*, 9942-9943.

- (17) Jahn, H.A.; Teller, E. Stability of Polyatomic Molecules in Degenerate Electronic States I-Orbital Degeneracy. *Proc. Roy. Soc. (London).* **1937**, *161-A*, 220-235.
- (18) Belluz, P.D.B.; Cordes, A.W.; Kristof, E.M.; Kristof, P.V.; Liblong, S.W.; Oakley, R.T. 1,2,3,5-diselenadiazolyls as Building Blocks for Molecular Metals. Preparation and Structures of  $[PhCN_2Se_2]^+PF6^-$  and  $[PhCN_2Se_2]_2$ . *J. Am. Chem. Soc.* 1989, 111, 9276-9278.
- (19) West, A.R. Solid State Chemistry and its Applications Student Edition, 2nd ed.; John Wiley & Sons Ltd: West Sussex, 2014.
- (20) Ferrais, J.; Cowan, D.O.; Walatka Jr., V.; Perlstein, J.H. Electron Transfer in a New Highly Conducting Donor-Acceptor Complex. 1973, 95, 948-949.

- (21) Solovyeva, V.; Huth, M. Defect-induced shift of the Peierls transition in TTF-TCNQ thin films. *Synth. Met.* **2011**, *161*, 976-983.
- (22) Bryan, C.D.; Cordes, A.W.; Fleming, R.M.; George, N.A.; Glarum, S.H.; Haddon, R.C.; Oakley, R.T.; Palstra, T.T.M.; Perel, A.S.; Schneemeyer, L.F.; Waszczak, J.V. Conducting charge-transfer salts based on neutral pi-radicals. *Nature*, 1993, 365, 821-823.
- (23) Cordes, A.W.; Haddon, R.C.; Oakley, R.T. Molecular Conductors from Neutral Heterocyclic pi-radicals. *Adv. Mater.* **1994**, *6*, 798-802.
- (24) Harris, P.M.; Mack, E.; Blake, F.C. The Atomic Arrangement in the Crystal of Orthorhombic Iodine. *J. Am. Chem. Soc.* **1928**, 50, 1583-1600.